Available online at www.sciencedirect.com
SCIENCE DIRECT
ELSEVIER Computers and Mathematics with Applications 48 (2004) 1677–1692
An International Journal
computers & mathematics with applications
www.elsevier.com/locate/camwa

Genuinely Nonlinear Models for Convection-Dominated Problems

T. ILIESCU
Department of Mathematics, Virginia Polytechnic Institute and State University
456 McBryde Hall, Blacksburg, VA 24061-0123, U.S.A.

(Received October 2002; revised and accepted October 2003)

Abstract—This paper introduces a general, nonlinear subgrid-scale (SGS) model, having *bounded* artificial viscosity, for the numerical simulation of convection-dominated problems. We also present a numerical comparison (error analysis and numerical experiments) between this model and the most common SGS model of Smagorinsky, which uses a p-Laplacian regularization. The numerical experiments for the 2-D convection-dominated convection-diffusion test problem show a clear improvement in solution quality for the new SGS model. This improvement is consistent with the bounded amount of artificial viscosity introduced by the new SGS model in the sharp transition regions.

Keywords—Subgrid-scale model, Artificial viscosity, p-Laplacian.

1. INTRODUCTION

One of the fundamental difficulties in the numerical study of convection-dominated problems is that considerable information can be contained in small scales, below the level of the finest mesh. To represent these effects on the larger scales, different methodologies have been used in practical calculations. These methodologies have been successfully analyzed and implemented in the linear case of convection-diffusion problems (the streamline-diffusion method is probably the most successful in this class). For nonlinear problems (e.g., the Navier-Stokes equations), one of the most common methodologies is to use various subgrid-scale (SGS) models (see, e.g., [1–3], for a survey of these models). However, very little rigorous mathematical analysis has been done validating the effects of these nonlinear SGS terms on the underlying continuum model and on the discretization ultimately employed.

The goal of this paper is twofold. First, we introduce a general, nonlinear SGS model, having *bounded* artificial viscosity. Then, we start a careful comparison of this new SGS model with the most common SGS model of Smagorinsky [4], which uses a p-Laplacian regularization. Specifically, we present the error analysis for the corresponding finite element method (FEM)

This work was supported in part by the Mathematical, Information, and Computational Sciences Division subprogram of the Office of Advanced Scientific Computing Research, U.S. Department of Energy, under Contract W-31-109-Eng-38, and by NSF Grant DMS-0209309.
I thank W.J. Layton for generously bringing this problem to my attention, and for his help and constant support in writing this paper. I also thank D. Ševčovič for his generous help in proving Lemma 3.2.

0898-1221/04/$ - see front matter Typeset by $\mathcal{A}\mathcal{M}\mathcal{S}$-TEX
doi:10.1016/j.camwa.2004.10.009

discretizations of the two SGS models, as well as numerical experiments for the 2-D convection-dominated convection-diffusion test problem with homogeneous Dirichlet boundary conditions

$$-\varepsilon\Delta u + \mathbf{b}\cdot\nabla u + cu = f, \qquad \text{in } \Omega, \tag{1}$$

$$u = 0, \qquad \text{on } \partial\Omega, \tag{2}$$

where Ω is a polyhedral domain in $\mathbb{R}^d$ $(d = 2, 3)$, $\mathbf{b} : \Omega \to \mathbb{R}^d$, $c : \Omega \to \mathbb{R}$, $f : \Omega \to \mathbb{R}$, and $0 < \varepsilon \ll 1$. This test problem is a first and essential step in careful numerical comparison of the two SGS models, in that there is little (if any) hope of understanding the effects of these SGS terms upon the discretization of more general, nonlinear problems (as the Navier-Stokes equations), without studying these effects on (1),(2), first.

The most common approach for the discretization of the linear problem (1),(2) is the streamline-diffusion finite element method (SDFEM). SDFEM, introduced by Hughes and Brooks [5], and mainly analyzed by Nävert [6,7] and Eriksson and Johnson [8], is a great improvement of the common upwind type methods and has been successfully implemented and tested on a wide variety of problems [9,10]. SDFEM stabilizes (1),(2) in a consistent way, introducing a linear amount of artificial viscosity (AV) in the direction of the flow, and reducing the need for extra stabilizing AV. Along these lines, a further way to reduce the need for extra stabilizing AV is to apply the AV locally, via a Smagorinsky-type SGS term of the form

$$-\nabla\left(\mu h^{\sigma}\left|h\nabla u^h\right|^{p-2}\nabla u^h\right), \tag{3}$$

added to the discretization of the left-hand side (LHS) of (1). In the above formula, $|\cdot|$ is the Euclidian norm, h represents the mesh-width in the discretization of (1),(2), u^h is the discretized solution, and μ, σ, and p are user-specified parameters. This extra *nonlinear* term introduces the AV in a *selective* way: it introduces a negligible amount of AV in smooth regions (where $|\nabla u^h|$ is small), and a stabilizing amount of AV in the sharp transition regions (where $|\nabla u^h| \sim O(h^{-1})$). The p-Laplacian AV term (3) stabilizes the discretization and also spreads the small (below the mesh-width) scales onto the computable mesh. This p-Laplacian AV term has been used in numerous challenging numerical applications; the Smagorinsky [4] model, which uses a p-Laplacian AV term, is one of the most popular models in the numerical simulation of turbulent flows [1–3]. However, very little rigorous analysis, mathematical or numerical, has been done validating the corresponding continuum and discretized models (see [11–13]).

In Section 2, using the p-Laplacian's strong monotonicity, Minty's lemma [14,15], and discrete inverse Sobolev's inequalities, we prove existence, uniqueness, max-norm stability, and *a priori* error estimates for u^h, the approximate solution of the discretization of (1),(2) including the nonlinear AV term (3). This analysis follows the approach used by Layton in [13] and complements the one on the pure p-Laplacian problem [16].

The p-Laplacian AV term (3), despite its well-known (see [13]) qualities, has the drawback of introducing an *unbounded* amount of AV in sharp transition regions, whereas just $O(h)$ AV is needed. Motivated by this drawback, we introduce in Section 3 a general, nonlinear, *bounded* AV term of the form

$$-\nabla\left(\mu h^{\sigma} a\left(\left|h\nabla u^h\right|\right)\nabla u^h\right), \tag{4}$$

added to the discretization of the LHS of (1). The parameters in (4) are the same as those in (3). The function $a(\cdot)$, however, instead of being a power function (and thus *unbounded*) as in the p-Laplacian AV term (3), is a general bounded, smooth, nonnegative, real-valued function, whose derivative is also bounded (see Figure 1).

The nonlinear AV term (4) introduces a bounded amount of AV in the sharp transition regions, and almost no AV in the smooth regions.

Since the nonlinear bounded AV term (4) has no monotonicity properties, the error analysis for the corresponding model is more challenging than the one for the p-Laplacian AV model. In

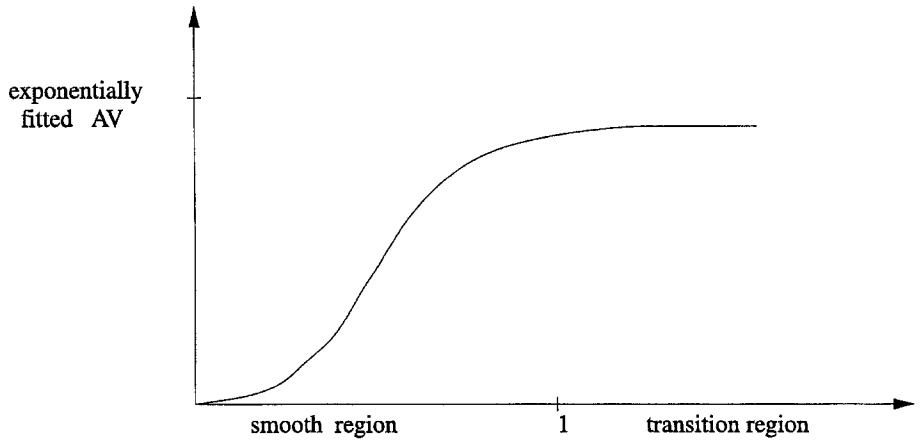

Figure 1. The graph of $a(\cdot)$; the horizontal axis represents $|h\nabla u^h|$.

Section 3, we prove existence, uniqueness, and *a priori* error estimates for u^h, the approximate solution of the discretization of (1),(2) including the nonlinear AV term (4).

Numerical experiments reported in Section 4 show that, for problems exhibiting very sharp layers, the bounded AV model shows a visible improvement in solution quality versus the p-Laplacian AV model.

These numerical experiments, supported by a careful mathematical and numerical analysis, which we begin here, make the bounded nonlinear AV SGS model a promising approach for the numerical study of convection-dominated problems, such as turbulent flows.

2. ERROR ANALYSIS FOR THE p-LAPLACIAN AV MODEL

We begin by introducing the mathematical structures needed for the numerical analysis of the p-Laplacian AV model. Let $\Pi^h(\Omega)$ denote the finite element partition of Ω into face-to-face d-simplices ($d = 2, 3$) with mesh-width (maximum d-simplex diameter) h. The minimum angle in $\Pi^h(\Omega)$, $\theta_{\min}$, is assumed to be bounded away from zero uniformly in h. The norm $\|\cdot\|$ denotes the usual $L^2(\Omega)$ norm, and $\|\cdot\|_{L^p}$ denotes the $L^p(\Omega)$ norm. The norm on $W^{-1,q}$, the dual of the Sobolev space $W_0^{1,p}$, is defined by

$$\|\Phi\|_{W^{-1,q}} := \sup_{0 \neq v \in W_0^{1,p}} \frac{(\Phi, v)}{\|\nabla v\|_{L^p}},$$

where $1/p + 1/q = 1$.

Let $X = H_0^1(\Omega)$, its norm $\|\cdot\|_X := \|\cdot\|_{1,\Omega}$, and $(\cdot,\cdot)$ the $L^2(\Omega)$ inner product. The usual weak formulation [9,17,18] of problem (1),(2) is to find $u \in X$ satisfying

$$\varepsilon(\nabla u, \nabla v) + (\mathbf{b} \cdot \nabla u, v) + (cu, v) = (f, v), \qquad \forall v \in X. \tag{5}$$

We define an energy-norm associated with (5)

$$|||v||| := \left(\varepsilon\|\nabla v\|^2 + \|v\|^2\right)^{1/2}.$$

The spaces X^h are associated conforming finite element spaces, $X^h \subset X$, and $B(\cdot,\cdot)$ represents the usual bilinear form associated with (5). Specifically, for $u, v \in X$

$$B(u, v) := \varepsilon(\nabla u, \nabla v) + (\mathbf{b} \cdot \nabla u, v) + (cu, v). \tag{6}$$

Using the Riesz representation theorem, define $AV_p : W_0^{1,p} \to (W_0^{1,p})'$ by

$$(AV_p(u), v) := \mu h^\sigma \left((|h\nabla u|)^{p-2} \nabla u, \nabla v \right), \qquad \forall u, v \in W_0^{1,p}, \tag{7}$$

with $\mu > 0$, $\sigma > 0$, and $p \geq 2$.

Since $AV_p(\cdot)$ is associated with the p-Laplacian, its monotonicity properties are documented in many places (see, e.g., [14,15]). We summarize them here,

$$(AV_p(u) - AV_p(v), u - v) \geq \mu C_1(p) h^{\sigma+p-2} \|\nabla(u - v)\|_{L^p}^p, \tag{8}$$

$$\|AV_p(u) - AV_p(v)\|_{W^{-1,q}} \leq \mu C_2(p) h^{\sigma+p-2} r^{p-2} \|\nabla(u - v)\|_{L^p}, \tag{9}$$

where $C_1(p)$ and $C_2(p)$ are constants independent of h, $r := \max\{\|\nabla u\|_{L^p}, \|\nabla v\|_{L^p}\}$, and $1/p + 1/q = 1$.

By a coercivity argument [10], there exists a unique solution of (5), provided that there exists a constant $\tilde{\alpha}$ such that

$$\inf_{\mathbf{x} \in \Omega} \left\{ c(\mathbf{x}) - \frac{1}{2} (\nabla \cdot \mathbf{b})(\mathbf{x}) \right\} \geq \tilde{\alpha} \geq 0. \tag{10}$$

We now begin the study of the p-Laplacian AV model for the convection-dominated convection-diffusion problem (1),(2), given by

$$\mu h^\sigma \left(\left| h\nabla u^h \right|^{p-2} \nabla u^h, \nabla v \right) + \varepsilon \left(\nabla u^h, \nabla v \right) + \left(\mathbf{b} \cdot \nabla u^h, v \right) + \left(c u^h, v \right) = (f, v), \qquad \forall v \in X^h. \tag{11}$$

Since the above model is nonlinear, it is not altogether obvious that an approximate solution u^h exists. The following lemma answers this question.

LEMMA 2.1. *(Existence and uniqueness of u^h.) There exists a unique solution for (11).*

PROOF. The proof follows from the coercivity of the bilinear form in (11), the strong monotonicity (8) of the p-Laplacian AV term, and Minty's lemma [14,15].

For the error analysis we will need to use discrete tools linking the $L^2(\Omega)$ and $L^p(\Omega)$ norms. In particular, most commonly used finite element spaces satisfy the following inverse inequality and Poincaré inequality:

$$C_1 h \|\nabla v\| \leq \|v\| \leq C_2 \|\nabla v\|, \qquad \forall v \in X^h, \tag{12}$$

where C_1, C_2 are constants independent of h. ∎

We will also need the following L^p-L^2-type inverse inequality [13, Lemma 2.1].

LEMMA 2.2. *Let $\theta_{\min}$ be the minimum angle in the triangulation and $M^k = \{v(x) : v \in C(\bar{\Omega}), v|_T \in P_k(T), \forall T \in \Pi^h(\Omega)\}$, P_k being the polynomials of degree $\leq k$. Then, there is a $C = C(\theta_{\min}, p, k)$ such that for $2 \leq p < \infty$, $d = 2, 3$, and all $v \in M^k$*

$$\|\nabla v\|_{L^p(\Omega)} \leq C h^{(d/2)((2-p)/p)} \|\nabla v\|. \tag{13}$$

A stability result for method (11) with p-Laplacian regularization is given by the following lemma.

LEMMA 2.3. *If $p > d$, then*

$$\|u^h\| \leq \frac{\|f\|}{C\varepsilon + \tilde{\alpha}}, \qquad \text{and} \tag{14}$$

$$\|u^h\|_{L^\infty} \leq C h^{-(\sigma+p-2)/(p-1)} \|f\|_{W^{-1,q}}^{1/(p-1)}, \tag{15}$$

where C is a generic constant independent of h.

PROOF. Setting $v = u^h$ in (11), we get

$$\mu h^{\sigma+p-2} \left\|\nabla u^h\right\|_{L^p}^p + B\left(u^h, u^h\right) = \left(f, u^h\right).$$

Using (10), (12), the above equality, and Hölder's inequality, we get

$$\begin{aligned} \left(C_2^{-2}\varepsilon + \tilde{\alpha}\right) \left\|u^h\right\|^2 &\leq \|f\| \left\|u^h\right\|, \qquad \text{and} \\ \mu h^{\sigma+p-2} \left\|\nabla u^h\right\|_{L^p}^p &\leq \|f\|_{W^{-1,q}} \left\|\nabla u^h\right\|_{L^p}, \end{aligned}$$

where $1/p + 1/q = 1$. Therefore,

$$\left\|u^h\right\| \leq \frac{\|f\|}{C_2^{-2}\varepsilon + \tilde{\alpha}},$$

which proves (14), and

$$\mu h^{\sigma+p-2} \left\|\nabla u^h\right\|_{L^p}^{p-1} \leq \|f\|_{W^{-1,q}},$$

which implies

$$\left\|\nabla u^h\right\|_{L^p} \leq \mu^{-1/(p-1)} h^{-(\sigma+p-2)/(p-1)} \|f\|_{W^{-1,q}}^{1/(p-1)}.$$

By the Sobolev embedding theorem, we have that, for $p > d$,

$$\left\|u^h\right\|_{L^\infty} < C(\Omega) \left\|\nabla u^h\right\|_{L^p}.$$

From the above two inequalities, (15) now follows. ∎

2.1. *A Priori* Error Analysis

An *a priori* error estimate for method (11) is given by the following theorem.

THEOREM 2.1. *Suppose that X^h satisfies estimate (13) and that $\inf_{w \in X^h} \|\nabla w\|_{L^p} \leq C\|\nabla u\|$. Then,*

$$\begin{aligned} &\mu C h^{\sigma+p-2} \left\|\nabla\left(u - u^h\right)\right\|_{L^p}^p + \varepsilon \left\|\nabla\left(u - u^h\right)\right\|^2 + \left\|u - u^h\right\|^2 \\ &\leq C \inf_{w \in X^h} \Big\{ \|u - w\|^2 + \varepsilon \|\nabla(u - w)\|^2 + \|\nabla(u - w)\|^2 + \mu h^{\sigma+p-2} \|\nabla(u - w)\|_{L^p}^p \\ &\qquad + \mu^2 \varepsilon^{-1} h^{2\sigma+2(p-2)+d((2-p)/p)} \|\nabla(u - w)\|_{L^p}^2 \|\nabla u\|_{L^p}^{2(p-2)} \Big\} \\ &\qquad + \mu^2 C \varepsilon^{-1} h^{2\sigma+2(p-2)+d((2-p)/p)} \|\nabla u\|_{L^p}^{2p-2}, \end{aligned}$$

where C is a generic constant independent of h.

PROOF. The error bound is proved by using Galerkin orthogonality and the monotonicity of $AV_p(\cdot)$ (8). First, the error equation is derived. Subtracting (11) from (5), we get

$$-\left(AV_p\left(u^h\right), v\right) + B(e, v) = 0, \qquad \forall v \in X^h, \tag{16}$$

where $e = u - u^h$. Let $w \in X^h$ be arbitrary and define $\phi = w - u^h \in X^h$, $\eta = u - w$ (note that $e = \eta + \phi$). Adding and subtracting terms as appropriate and using the bilinearity of $B(\cdot, \cdot)$, we get

$$\begin{aligned} (AV_p(w), v) - \left(AV_p\left(u^h\right), v\right) + B(\phi, v) &= (AV_p(w), v) - (AV_p(u), v) \\ -B(\eta, v) + (AV_p(u), v), \qquad \forall v \in X^h. \end{aligned} \tag{17}$$

Using (9), we also have

$$\begin{aligned} (AV_p(u), v) = (AV_p(u), v) - (AV_p(0), v) &\leq \|AV_p(u) - AV_p(0)\|_{W^{-1,2}} \|\nabla v\| \\ &\leq \mu C_2(p) h^{\sigma+p-2} \|\nabla u\|_{L^p}^{p-1} \|\nabla v\|. \end{aligned} \tag{18}$$

If we set $v = \phi$ (since $\phi \in X^h$) and use the strong monotonicity of $AV_p(\cdot)$ (8) and the coercivity of $B(\cdot,\cdot)$ on the LHS of (17), the local-Lipschitz continuity of $AV_p(\cdot)$ (9) and the continuity of $B(\cdot,\cdot)$ on the right-hand side (RHS), and (18), we obtain

$$\begin{aligned}\mu C_1(p) h^{\sigma+p-2} \|\nabla\phi\|_{L^p}^p + \varepsilon\|\nabla\phi\|^2 + \tilde{\alpha}\|\phi\|^2 \leq \mu C_2(p) h^{\sigma+p-2} r^{p-2} \|\nabla\phi\|_{L^p} \|\nabla\eta\|_{L^p} + \varepsilon\|\nabla\eta\| \, \|\nabla\phi\| \\ + K_1\|\nabla\eta\| \, \|\phi\| + K_2\|\eta\| \, \|\phi\| \\ + \mu C_2(p) h^{\sigma+p-2} \|\nabla u\|_{L^p}^{p-1} \|\nabla\phi\|_{L^p},\end{aligned}$$

where $r = \max\{\|\nabla u\|_{L^p}, \|\nabla w\|_{L^p}\}$.

Using Lemma 2.2 and the Cauchy-Schwarz inequality on the RHS yields

$$\begin{aligned}\mu h^{\sigma+p-2} C_1(p) \|\nabla\phi\|_{L^p}^p + C\varepsilon\|\nabla\phi\|^2 + C\|\phi\|^2 \leq \mu^2 C(p) \varepsilon^{-1} r^{2(p-2)} h^{2\sigma+2(p-2)+d((2-p)/p)} \|\nabla\eta\|_{L^p}^2 \\ + \mu^2 C(p) \varepsilon^{-1} h^{2\sigma+2(p-2)+d((2-p)/p)} \|\nabla u\|_{L^p}^{2p-2} \\ + C\varepsilon\|\nabla\eta\|^2 + C\|\nabla\eta\|^2.\end{aligned}$$

Since $\|u_1+u_2\|_{L^p}^p \leq C(p)(\|u_1\|_{L^p}^p + \|u_2\|_{L^p}^p)$, and $r \leq C\|\nabla u\|_{L^p}$ at infimum, the result now follows taking the infimum over $w \in X^h$ of the above inequality and using the triangle inequality. ∎

REMARK 2.1. L^p stability of the L^2 projection into finite element spaces is proved in [19].

REMARK 2.2. Theorem 2.1 also proves the convergence of u^h. Indeed, since $\sigma > 0$, $p \geq 2$, and $d = 2, 3$, we get $2\sigma + 2(p-2) + d(d-p)/p > 0$.

REMARK 2.3. The convergence of u^h is not uniform in ε. However, for many practical choices of the parameters σ and p, the scaling between ε and h is reasonable. For example, in 2-D ($d = 2$), for $p \geq 3$ and $\sigma \geq 1$, we have $2\sigma + (p-2)(2-2/p) \geq 10/3$, and thus $\varepsilon > O(h^{10/3})$, in order to get convergence of u^h. In 3-D ($d = 3$), for $p \geq 3$ and $\sigma \geq 1$, we have $2\sigma + (p-2)(2-2/p) \geq 3$, and thus $\varepsilon > O(h^3)$ in order to get convergence of u^h.

3. ERROR ANALYSIS FOR THE GENERAL BOUNDED AV MODEL

In this section, we study the general, bounded AV model used for the discretization of the convection-dominated convection-diffusion problem (1),(2)

$$\mu h^\sigma \left(a\left(\left|h\nabla u^h\right|\right)\nabla u^h, \nabla v\right) + \varepsilon\left(\nabla u^h, \nabla v\right) + \left(\mathbf{b}\cdot\nabla u^h, v\right) + \left(cu^h, v\right) = (f, v), \qquad \forall v \in X^h. \tag{19}$$

We start with a very general AV model (i.e., a very general function $a(\cdot)$), and then we impose restrictions on it in order to obtain existence, uniqueness, and convergence for the solution of the discretized problem. In particular, we prove an *a priori* error bound for u^h, the approximate solution of (19).

Here, $\sigma > 0$ and $\mu > 0$ are parameters to be determined, and $a(\cdot)$ is a smooth, bounded, nonnegative function whose graph looks like that in Figure 1.

The shape of $a(\cdot)$ makes the AV term $\mu h^\sigma(a(|h\nabla u^h|)\nabla u^h, \nabla v)$ fit the description we gave in the introduction: the amount of AV introduced in the discretization (19) is negligible in the smooth regions (where the gradient is small) and bounded where the gradient is large

$$\mu h^\sigma\left(\left|h\nabla u^h\right|^{p-2}\nabla u^h, \nabla v\right) \sim \begin{cases} h^\sigma\left(\nabla u^h, \nabla v\right), & \text{where } \left|\nabla u^h\right| \sim O\left(h^{-1}\right), \\ h^{p+\sigma-2}\left(\nabla u^h, \nabla v\right), & \text{where } \left|\nabla u^h\right| \sim O(1). \end{cases}$$

We now seek conditions upon $a(\cdot)$ and μ, sufficient for the existence, uniqueness, and convergence of u^h.

LEMMA 3.1. *(Existence of u^h.) Assume that $\mathbf{b}(\cdot)$ and $c(\cdot)$ are smooth enough functions and that (10) is satisfied.*

Then, provided $a(\cdot) \geq 0$, there exists a solution to (19), and we have the following a priori bound:

$$\left\|u^h\right\|_1 \leq C(f,\varepsilon,h) := \frac{\|f\|_{-1}}{\varepsilon/\left(1+C_2^2\right)+\tilde{\alpha}/\left(1+C_1^{-2}h^{-2}\right)}, \tag{20}$$

where C_1, C_2 are constants independent of h.

REMARK 3.1. Condition (10) is a common condition that ensures existence and uniqueness of u, the solution of the continuous problem (5).

PROOF. Since $\dim(X^h) < \infty$, existence will follow from Schauder's fixed point theorem once we have proved an *a priori* bound on any *possible* solution u^h.

Using (12), we get

$$\left\|\nabla u^h\right\|^2 \geq \frac{\left\|u^h\right\|_1^2}{1+C_2^2}, \qquad \text{and} \qquad \left\|u^h\right\|^2 \geq \frac{\left\|u^h\right\|_1^2}{1+C_1^{-2}h^{-2}}, \tag{21}$$

where C_1, C_2 are constants independent of h.

Letting $v = u^h$ in (19) yields

$$\mu h^\sigma \left(a\left(\left|h\nabla u^h\right|\right)\nabla u^h, \nabla u^h\right) + \varepsilon\left(\nabla u^h, \nabla u^h\right) + \left(\mathbf{b}\cdot\nabla u^h, u^h\right) + \left(cu^h, u^h\right) = \left(f, u^h\right). \tag{22}$$

Since $a(\cdot)$ is nonnegative and $\mu > 0$, we have

$$\mu h^\sigma \left(a\left(\left|h\nabla u^h\right|\right)\nabla u^h, \nabla u^h\right) \geq 0.$$

Integrating by parts, using (10) and the above inequality on the LHS, and the Cauchy-Schwarz inequality on the RHS of (22), we have

$$\varepsilon\left\|\nabla u^h\right\|^2 + \tilde{\alpha}\left\|u^h\right\|^2 \leq \|f\|_{-1}\left\|u^h\right\|_1.$$

Using (21) in the above inequality, we get

$$\left(\frac{\varepsilon}{1+C_2^2} + \frac{\tilde{\alpha}}{1+C_1^{-2}h^{-2}}\right)\left\|u^h\right\|_1^2 \leq \|f\|_{-1}\left\|u^h\right\|_1, \tag{23}$$

which yields (20). Estimate (20) and Schauder's fixed point theorem prove existence of u^h, the solution to (19). ∎

REMARK 3.2. Notice that for the existence of u^h, we did not impose any new conditions on $a(\cdot)$ (other than those already imposed in the beginning of the section) or on μ. Thus, any function $a(\cdot)$ whose graph resembles the one in Figure 1 is admissible.

The following proposition proves the uniqueness of u^h, with a very general condition on $a(\cdot)$. Note that usually the uniqueness is proved by means of monotonicity arguments. These arguments fail in this case, and we have to use nontrivial nonlinear variational analysis arguments [15] instead.

LEMMA 3.2. *(Uniqueness of u^h.) Assume that the conditions in Lemma 2.2 are satisfied and that*

$$a'(x) \geq 0, \qquad \forall\, x \geq 0. \tag{24}$$

Then, there exists a unique solution u^h to (19).

PROOF. Assume there are two solutions u_1^h, u_2^h in X^h. Subtracting the two corresponding equations, we get

$$\begin{aligned}\mu h^\sigma &\left(a\left(\left|h\nabla u_1^h\right|\right)\nabla u_1^h - a\left(\left|h\nabla u_2^h\right|\right)\nabla u_2^h, \nabla v\right) + \varepsilon\left(\nabla u_1^h - \nabla u_2^h, \nabla v\right) \\ &+ \left(\mathbf{b}\cdot\nabla u_1^h - \mathbf{b}\cdot\nabla u_2^h, v\right) + \left(cu_1^h - cu_2^h, v\right) = 0, \qquad \forall\, v \in X^h.\end{aligned}$$

Letting $v := u_1^h - u_2^h \in X^h$, integrating by parts, and using (10) in the above equation, we have

$$\begin{aligned}\mu h^\sigma \left(a\left(\left|h\nabla u_1^h\right|\right)\nabla u_1^h - a\left(\left|h\nabla u_2^h\right|\right)\nabla u_2^h, \nabla\left(u_1^h - u_2^h\right)\right)\\ +\varepsilon\left\|\nabla\left(u_1^h - u_2^h\right)\right\|^2 + \tilde{\alpha}\left\|\left(u_1^h - u_2^h\right)\right\|^2 \le 0.\end{aligned} \tag{25}$$

The first term in the above inequality can be rewritten as

$$\frac{\mu h^\sigma}{h^2}\left(a\left(\left|h\nabla u_1^h\right|\right)h\nabla u_1^h - a\left(\left|h\nabla u_2^h\right|\right)h\nabla u_2^h, h\nabla\left(u_1^h - u_2^h\right)\right). \tag{26}$$

Consider now the following functional:

$$I : H^1(\Omega) \to \mathbb{R}, \qquad I(U) := \int_\Omega A(|\nabla U(\mathbf{x})|)\,d\mathbf{x},$$

where

$$A : [0,\infty) \to \mathbb{R}, \qquad A(x) = \int_0^x ta(t)\,dt.$$

Notice that

$$dI(U,V) = \int_\Omega A'(|\nabla U|)\frac{\nabla U}{|\nabla U|}\nabla V\,d\mathbf{x} = \int_\Omega a(|\nabla U|)\nabla U\nabla V\,d\mathbf{x},$$

where $dI(U,V)$ is the Gâteaux derivative of I at U in the direction V.

Letting $U_1 := hu_1$, $U_2 := hu_2$, and $V := U_1 - U_2$, (26) reads

$$\frac{\mu h^\sigma}{h^2}(dI(U_1,V) - dI(U_2,V)),$$

which is equal to

$$\begin{aligned}&\frac{\mu h^\sigma}{h^2}\int_0^1 \frac{d}{dt}dI(U_2 + t(U_1 - U_2), V)\,dt\\ &\quad= \frac{\mu h^\sigma}{h^2}\int_0^1 \frac{d}{dt}\int_\Omega a(|\nabla(U_2 + t(U_1 - U_2))|)\nabla(U_2 + t(U_1 - U_2))\nabla V\,d\mathbf{x}\,dt\\ &\quad= \frac{\mu h^\sigma}{h^2}\int_0^1\int_\Omega a'(|\nabla(U_2 + t(U_1 - U_2))|)\frac{\nabla(U_2 + t(U_1 - U_2))\nabla V}{|\nabla(U_2 + t(U_1 - U_2))|}\nabla(U_2 + t(U_1 - U_2))\nabla V\\ &\qquad+ a(|\nabla(U_2 + t(U_1 - U_2))|)|\nabla V|^2\,d\mathbf{x}\,dt.\end{aligned}$$

Since $a'(x) \ge 0$, $\forall x \ge 0$ by (24), and $a(x) \ge 0$, $\forall x \ge 0$, the above expression is nonnegative. Thus, (26) is nonnegative; nonnegativity of (26) and (25) implies

$$\varepsilon\left\|\nabla\left(u_1^h - u_2^h\right)\right\|^2 + \tilde{\alpha}\left\|\left(u_1^h - u_2^h\right)\right\|^2 \le 0.$$

Therefore, since $\varepsilon > 0$, $\tilde{\alpha} \ge 0$, and $u_1^h - u_2^h \in X^h \subseteq H_0^1(\Omega)$, we get

$$u_1^h = u_2^h. \qquad \blacksquare$$

REMARK 3.3. Note that condition (24) is satisfied by any function $a(\cdot)$ whose graph resembles the one in Figure 1.

3.1. *A Priori* Error Analysis

In this section, we present the *a priori* error analysis for the approximate solution u^h. For a very general function $a(\cdot)$, this *a priori* error analysis is summarized in the following theorem.

THEOREM 3.1. *Assume that $a(\cdot)$ is a positive, increasing function and that $\mathbf{b}(\cdot)$ and $c(\cdot)$ are continuous on $\bar{\Omega}$. Further suppose*

$$a(x) \leq 1, \qquad \forall\, x \geq 0. \tag{27}$$

Then, we have the following a priori estimate:

$$\begin{aligned}
&\frac{\varepsilon}{8}\left\|\nabla\left(u-u^h\right)\right\|^2+\frac{\tilde{\alpha}}{4}\left\|\left(u-u^h\right)\right\|^2 \\
&\leq \inf_{w\in X^h}\left\{\left(\frac{3\varepsilon}{4}+\frac{K_1}{\tilde{\alpha}}\right)\|\nabla(w-u)\|^2+\left(\frac{K_2}{\tilde{\alpha}}+\frac{\tilde{\alpha}}{2}\right)\|w-u\|^2\right\} \\
&+\frac{1}{\varepsilon}\left(\frac{\mu h^\sigma\|f\|_{-1}}{\varepsilon\left(\sqrt{1+C_1^2h^2}/\left(1+C_2^2\right)\right)+\tilde{\alpha}C_1^2h^2/\sqrt{1+C_1^2h^2}}\right)^2,
\end{aligned}$$

where C_1, C_2, K_1, K_2 are constants independent of h, and $\tilde{\alpha}$ is the constant given by (10).

PROOF. Subtracting (19) from (5), and using the fact that $X^h \subseteq X$, we get

$$-\mu h^\sigma\left(a\left(\left|h\nabla u^h\right|\right)\nabla u^h,\nabla v\right)+\varepsilon\left(\nabla\left(u-u^h\right),\nabla v\right)+\left(\mathbf{b}\cdot\nabla\left(u-u^h\right)+c\left(u-u^h\right),v\right)=0, \qquad \forall\, v\in X^h.$$

Let $w \in X^h$. Set $e := u-u^h$, $\eta = w-u$, $\varphi = w-u^h \in X^h$, and notice that $e = \varphi - \eta$. Therefore, the above equation reads

$$\varepsilon(\nabla\varphi,\nabla v)+(\mathbf{b}\cdot\nabla\varphi+c\varphi,v)=\varepsilon(\nabla\eta,\nabla v)+(\mathbf{b}\cdot\nabla\eta+c\eta,v)+\mu h^\sigma\left(a\left(h\left|\nabla u^h\right|\right)\nabla u^h,\nabla v\right).$$

Setting $v=\varphi$ yields

$$\varepsilon\|\nabla\varphi\|^2+(\mathbf{b}\cdot\nabla\varphi+c\varphi,\varphi)=\varepsilon(\nabla\eta,\nabla\varphi)+(\mathbf{b}\cdot\nabla\eta+c\eta,\varphi)+\mu h^\sigma\left(a\left(\left|h\nabla u^h\right|\right)\nabla u^h,\nabla\varphi\right).$$

Integrating by parts and using (10) on the LHS, and the Cauchy-Schwarz inequality on the RHS, we have

$$\begin{aligned}
\varepsilon\|\nabla\varphi\|^2+\tilde{\alpha}\|\varphi\|^2 \leq{}& \frac{\varepsilon}{2}\|\nabla\eta\|^2+\frac{\varepsilon}{2}\|\nabla\varphi\|^2+\frac{1}{\tilde{\alpha}}\|\mathbf{b}\cdot\nabla\eta\|^2+\frac{\tilde{\alpha}}{4}\|\varphi\|^2+\frac{1}{\tilde{\alpha}}\|c\eta\|^2+\frac{\tilde{\alpha}}{4}\|\varphi\|^2 \\
&+\frac{1}{\varepsilon}\left(\mu^2h^{2\sigma}a\left(\left|h\nabla u^h\right|\right)\left\|\nabla u^h\right\|^2+\frac{\varepsilon}{4}\|\nabla\varphi\|^2.
\end{aligned}$$

Notice that the functions $\mathbf{b}(\cdot)$ and $c(\cdot)$ are continuous on $\bar{\Omega}$ (by hypothesis) and therefore bounded. Using this remark and (27), we have

$$\begin{aligned}
\varepsilon\|\nabla\varphi\|^2+\tilde{\alpha}\|\varphi\|^2 \leq{}& \frac{\varepsilon}{2}\|\nabla\eta\|^2+\frac{\varepsilon}{2}\|\nabla\varphi\|^2+\frac{K_1}{\tilde{\alpha}}\|\nabla\eta\|^2+\frac{\tilde{\alpha}}{4}\|\varphi\|^2+\frac{K_2}{\tilde{\alpha}}\|\eta\|^2+\frac{\tilde{\alpha}}{4}\|\varphi\|^2 \\
&+\frac{1}{\varepsilon}\mu^2h^{2\sigma}\left\|\nabla u^h\right\|^2+\frac{\varepsilon}{4}\|\nabla\varphi\|^2,
\end{aligned} \tag{28}$$

where K_1, K_2 are constants independent of h. Using (12) and (23) yields

$$\left\|\nabla u^h\right\| \leq \frac{\|f\|_{-1}}{\varepsilon\left(\sqrt{1+C_1^2h^2}/\left(1+C_2^2\right)\right)+\tilde{\alpha}C_1^2h^2/\sqrt{1+C_1^2h^2}}.$$

Thus, (28) becomes

$$\begin{aligned}
\frac{\varepsilon}{4}\|\nabla\varphi\|^2+\frac{\tilde{\alpha}}{2}\|\varphi\|^2 \leq{}& \frac{\varepsilon}{2}\|\nabla\eta\|^2+\frac{K_1}{\tilde{\alpha}}\|\nabla\eta\|^2+\frac{K_2}{\tilde{\alpha}}\|\eta\|^2 \\
&+\frac{1}{\varepsilon}\left(\frac{\mu h^\sigma\|f\|_{-1}}{\varepsilon\left(\sqrt{1+C_1^2h^2}/\left(1+C_2^2\right)\right)+\tilde{\alpha}C_1^2h^2/\sqrt{1+C_1^2h^2}}\right)^2.
\end{aligned}$$

By the triangle inequality, we get

$$\frac{1}{2}\left(\frac{\varepsilon}{4}\|\nabla(\varphi-\eta)\|^2+\frac{\tilde{\alpha}}{2}\|(\varphi-\eta)\|^2\right)\leq\frac{3\varepsilon}{4}\|\nabla\eta\|^2+\frac{K_1}{\tilde{\alpha}}\|\nabla\eta\|^2+\left(\frac{K_2}{\tilde{\alpha}}+\frac{\tilde{\alpha}}{2}\right)\|\eta\|^2 + \frac{1}{\varepsilon}\left(\frac{\mu h^\sigma\|f\|_{-1}}{\varepsilon\left(\sqrt{1+C_1^2h^2}/(1+C_2^2)\right)+\tilde{\alpha}C_1^2h^2/\sqrt{1+C_1^2h^2}}\right)^2.$$

Notice that $e=\varphi-\eta=u-u^h$ does not depend on w; thus, taking the infimum on w of both sides of the above inequality proves the theorem. ∎

REMARK 3.4. The *a priori* error estimate in Theorem 3.1 gives convergence of the approximate solution u^h to the exact solution u. The convergence is not uniform in ε. However, by choosing $a(\cdot)$ suitably, the discretization can be made to be exponentially fitted in all transition regions. Thus, an attempt to prove uniform in ε convergence would be legitimate in this case.

REMARK 3.5. Inequality (27) is satisfied by any function whose graph resembles the one in Figure 1, and allows us to introduce only $O(h^\sigma)$ AV in the sharp transition regions.

Summarizing the results in this section, for any parameters $\mu\geq 0$ and $\sigma\geq 0$, and for any smooth function $a(\cdot)$ satisfying

$$0\leq a(x)\leq 1,\qquad \forall x\geq 0,$$
$$0\leq a'(x),\qquad \forall x\geq 0,$$

we proved existence, uniqueness, and convergence for the solution u^h of (19). Notice that although our results hold true for a more general function $a(\cdot)$ satisfying the above relations, in practice we use a function whose graph resembles the one in Figure 1, introducing a negligible amount of AV in the smooth regions, and only $O(h^\sigma)$ in the sharp transition regions.

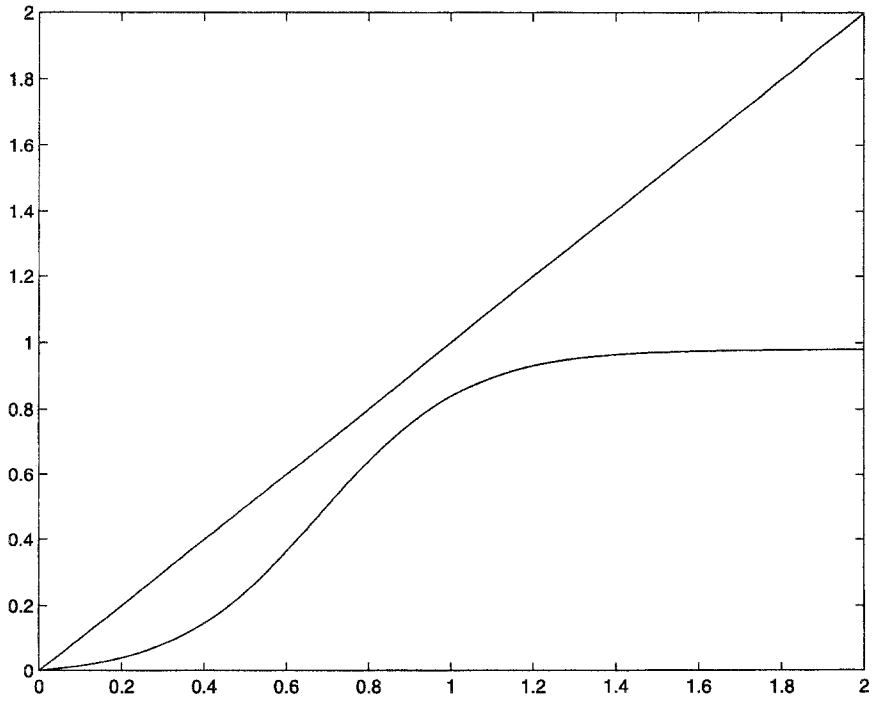

Figure 2. The graphs of $a(|h\nabla u^h|)$ and $|h\nabla u^h|$; the horizontal axis represents $|h\nabla u^h|$.

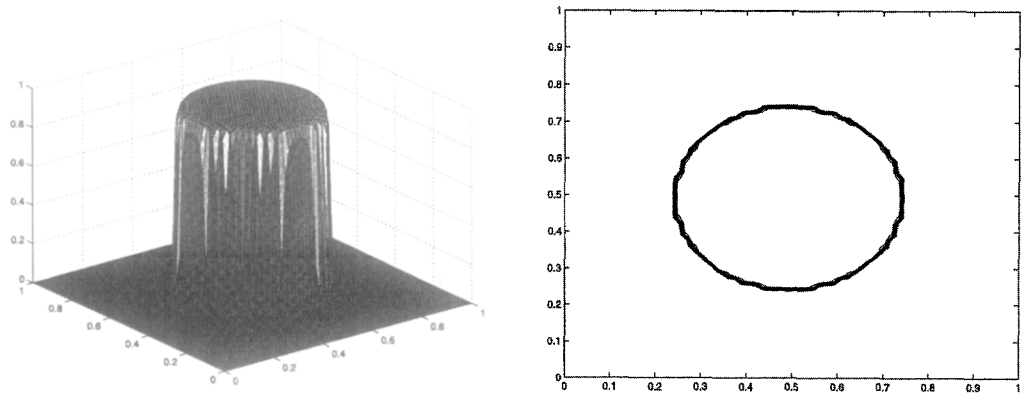

Figure 3. Example 1, the exact solution: surface plot and contour lines, $h = 1/64$.

4. NUMERICAL EXPERIMENTS

In this section, we present numerical tests for the SDFEM, the p-Laplacian AV SGS method, and the bounded AV SGS method. All three methods are applied to two challenging problems with sharp layers. These problems are catastrophically structurally unstable (small perturbations in the data result in dramatic unphysical oscillations, overshooting, and undershooting in the approximate solution), a characteristic feature of more general nonlinear flows (e.g., turbulent flows).

The boundary value problem (1),(2) is solved on the unit square $\Omega = (0,1) \times (0,1)$ by using a finite element discretization with conforming piecewise quadratics on a uniform mesh of isosceles right-angled triangles, with mesh-width h. The nonlinear problems (11) and (19) were solved by using a Picard-type iterative process (at each iteration we lagged the nonlinear term). All the matrices and the corresponding right-hand sides were assembled by using a second-order quadrature rule, and the resulting linear systems were solved by using the conjugate gradient squared (CGS) method [20].

EXAMPLE 1. This problem is a slight modification of the one used as a benchmark in [21] and has as the exact solution a circular blob (see Figure 3) with extremely sharp layers. We made the following parameter choices in (1),(2): $\varepsilon = 10^{-3}$, $c = 2$. The convection field was chosen as

$$\mathbf{b}(x,y) = \left(-(2y-1)\left(r_0^2 - (x-x_0)^2 - (y-y_0)^2\right), (2x-1)\left(r_0^2 - (x-x_0)^2 - (y-y_0)^2\right)\right),$$

for $0 \le (x-x_0)^2 - (y-y_0)^2 \le r_0^2$ and $\mathbf{b} = (0,0)$ otherwise, and the right-hand side and the boundary conditions were chosen such that

$$u(x,y) = \frac{1}{2} + \frac{\arctan\left[1000\left(r_0^2 - (x-x_0)^2 - (y-y_0)^2\right)\right]}{\pi},$$

with $x_0 = y_0 = 0.5$ and $r_0 = 0.25$, is the exact solution of (1),(2). Note that, even though our analysis considers the homogeneous problem (1),(2), the same analysis carries over in a straightforward way to the nonhomogeneous case.

First, we apply the usual SDFEM to problem (1),(2) [10],

$$\begin{aligned} \varepsilon\left(\nabla u^h, \nabla v\right) + \left(\mathbf{b}\cdot\nabla u^h, v\right) + \left(cu^h, v\right) + \sum_{T\in\Pi^h} \delta\left(-\varepsilon\Delta u^h + \mathbf{b}\cdot\nabla u^h + cu^h, \mathbf{b}\cdot\nabla v\right)_T \\ = (f,v) + \sum_{T\in\Pi^h} \delta(f, \mathbf{b}\cdot\nabla v)_T, \qquad \forall v \in X^h, \end{aligned} \tag{29}$$

where δ is a user-specified parameter. In our calculations, we used $\delta = h$, which is probably the most popular choice in SDFEM.

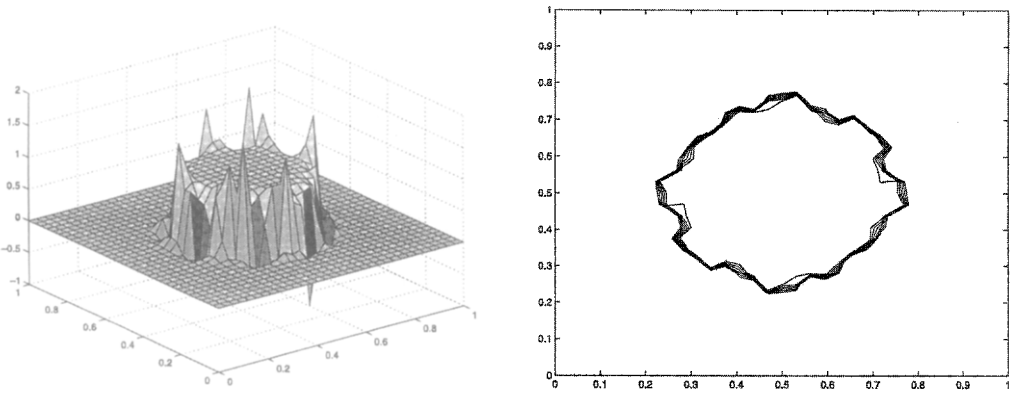

Figure 4. Example 1, the usual SDFEM: surface plot and contour lines, $\delta = h$, $h = 1/32$. Note the poor solution quality (smearing, overshooting, and undershooting).

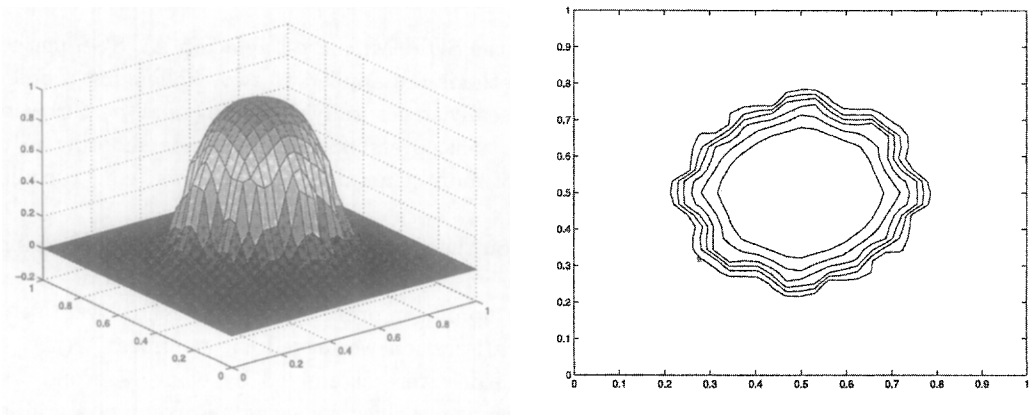

Figure 5. Example 1, the p-Laplacian AV SGS method: surface plot and contour lines; $\mu = 1$, $\sigma = 1$, $p = 3$, $h = 1/32$. Note the improvement in solution quality over Figure 4 (much smaller overshooting and undershooting).

The graph (surface plot and contour lines) of the corresponding approximation u^h is given in Figure 4. Note the poor solution quality: dramatic overshooting and undershooting.

Next, we apply the p-Laplacian AV SGS method (11) to (1),(2). Here, we used the following values for the user-specified parameters: $\mu = 1$, $\sigma = 1$, $p = 3$. The graph (surface plot and contour lines) of the corresponding approximation u^h is given in Figure 5. The p-Laplacian AV model introduces AV in a selective way (only in the sharp transition regions). This yields a visible improvement in solution quality (a clear reduction of the amount of overshooting and undershooting).

The last model tested is the general, bounded AV SGS model (19). For the user-specified parameters we made the following choices: $\mu = 1$, $\sigma = 2$, $a(t) = -0.02 + 1/(1 + 49e^{-5.7t})$. The choice of $a(\cdot)$ needs explanation. As mentioned at the end of Section 3, an "admissible" function $a(\cdot)$ should resemble the "S-shaped" graph in Figure 1 and should also introduce a nonnegligible amount is of AV only where $|\nabla u^h| \sim O(h^{-1})$. Thus, the user has to decide when exactly the gradient is "large", that is, for what value of $|h\nabla u^h|$ the value of $a(\cdot)$ should become nonnegligible. For this test problem, our choice was motivated by the parameter choice for the p-Laplacian AV term. For clarity, for the above parameter choices, we present in Figure 2 the graph of $a(\cdot)$ against the graph of the corresponding term in the p-Laplacian AV term (i.e., $|h\nabla u^h|$).

The graph (surface plot and contour lines) of the approximation u^h of the general, bounded

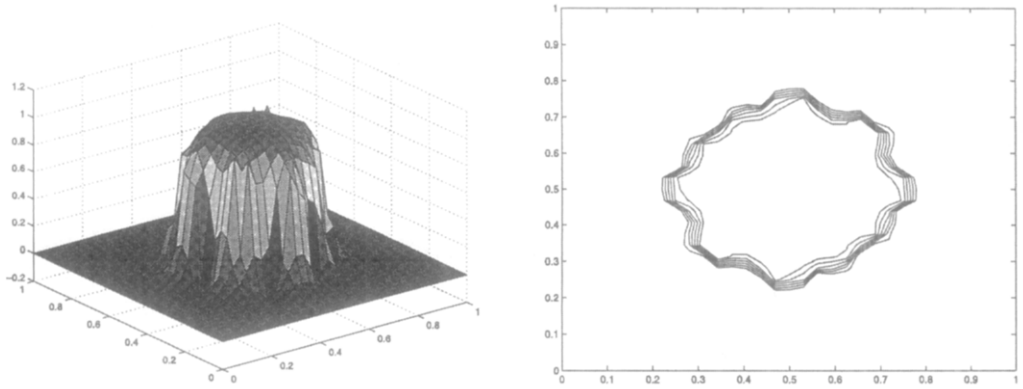

Figure 6. Example 1, the improved AV SGS method: surface plot and contour lines; $\mu = 1$, $\sigma = 2$, $a(t) = -0.02 + 1/(1 + 49e^{-5.7t})$, $h = 1/32$. Note the visible improvement over Figure 5 (sharper layer).

Table 1. Example 1, norms of the errors for the three different discretizations, where "E" represents the error. The bounded, nonlinear AV SGS model performs consistently better than the p-Laplacian AV SGS model.

h	Norm	SDFEM	p-Laplacian AV	Bounded AV
$\frac{1}{16}$	$\|E\|_{L^2}$	0.450+0	0.391+0	0.255+0
	$\|E\|_{H1}$	0.251+2	0.111+2	0.116+2
$\frac{1}{32}$	$\|E\|_{L^2}$	0.130+0	0.138+0	0.975−1
	$\|E\|_{H1}$	0.136+2	0.943+1	0.918+1
$\frac{1}{64}$	$\|E\|_{L^2}$	0.517−1	0.960−1	0.582−1
	$\|E\|_{H1}$	0.774+1	0.971+1	0.794+1
$\frac{1}{128}$	$\|E\|_{L^2}$	0.124−1	0.610−1	0.214−1
	$\|E\|_{H1}$	0.375+1	0.771+1	0.444+1

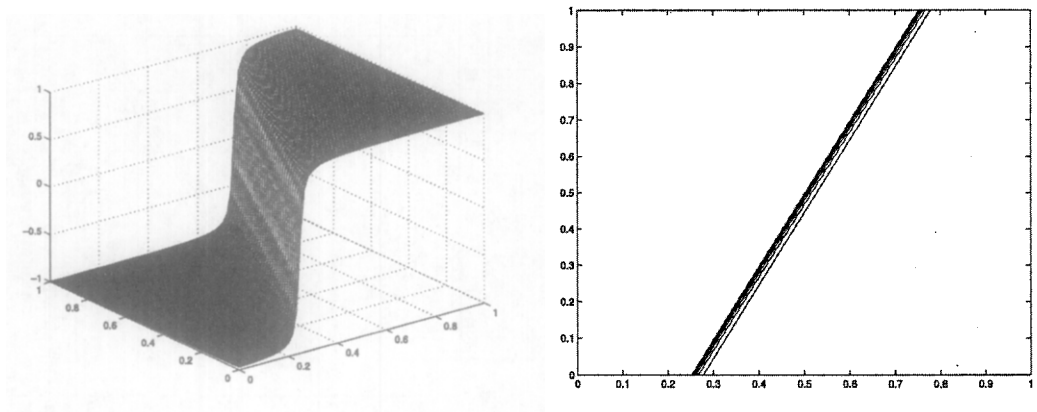

Figure 7. Example 2, the exact solution: surface plot and contour lines; $h = 1/64$.

AV model (19) is given in Figure 6. The solution quality is better than the one in Figure 5, in that the contour lines are much tighter. This improvement is due to the *bounded* amount of AV introduced by (19) in the sharp transition regions, just enough to spread the small scales on the resolvable mesh.

Since we know the exact solution, we can make more precise the above discussion and calculate the norm of the error in the three discretizations. In Table 1, for different mesh-widths ($h = 1/16$,

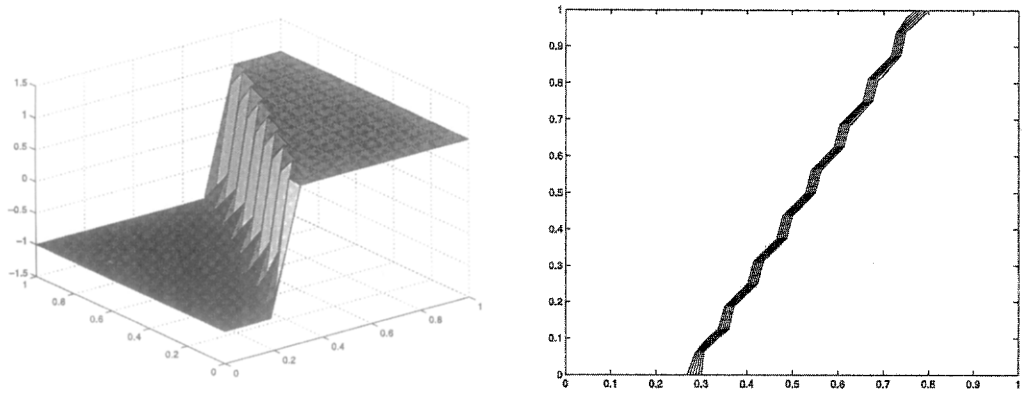

Figure 8. Example 2, the usual SDFEM: surface plot and contour lines; $\delta = h$, $h = 1/16$.

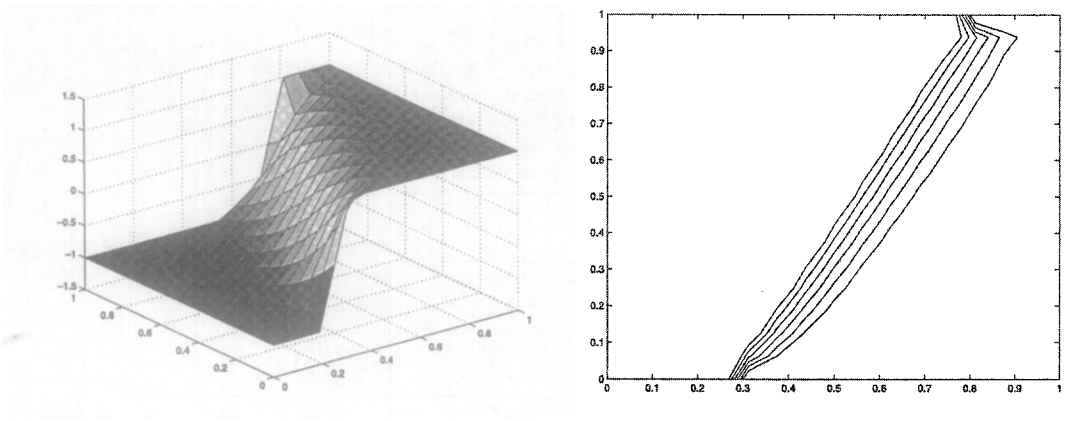

Figure 9. Example 2, the p-Laplacian AV SGS method: surface plot and contour lines; $\mu = 1$, $\sigma = 1$, $p = 3$, $h = 1/16$.

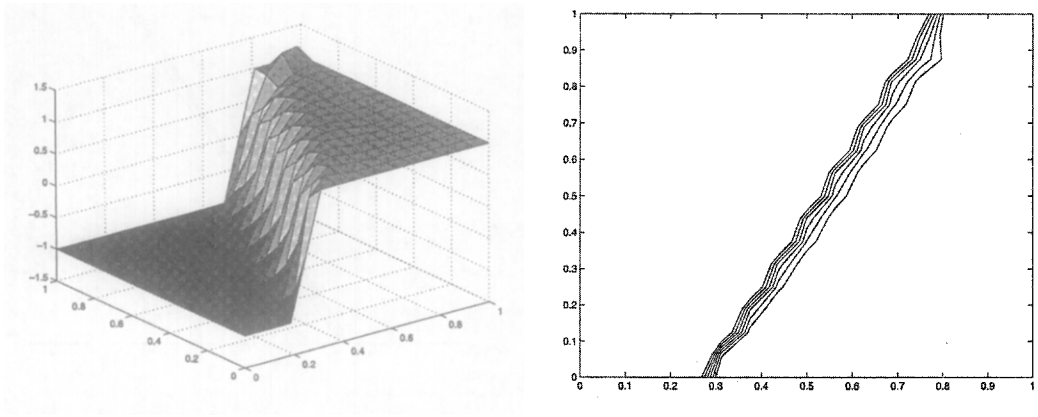

Figure 10. Example 2, the improved AV SGS method: surface plot and contour lines; $\mu = 1$, $\sigma = 2$, $a(t) = -0.02 + 1/(1 + 49e^{-5.7t})$, $h = 1/16$. Note the visible improvement over Figure 9 (sharper layer).

$h = 1/32$, $h = 1/64$, $h = 1/128$), we present the L^2-norm of the error (denoted by $\|E\|_{L^2}$), and the $H1$-seminorm of the error (denoted by $|E|_{H1}$).

The bounded AV model performs consistently better than the p-Laplacian AV model: for $h = 1/128$ the L^2 norm of the error is almost three times smaller for the bounded AV model.

Both nonlinear AV models perform better than the SDFEM for the coarse meshes ($h = 1/16$, $h = 1/32$), and worse for the finer meshes ($h = 1/64$, $h = 1/128$).

EXAMPLE 2. This problem, known as the "skew-step" problem, is a slight modification of the benchmark used in [21]. It has a steep internal layer, which makes it numerically unstable. In (1),(2), we made the following parameter choices: $\varepsilon = 10^{-3}$, $\mathbf{b} = (1, 0.5)$, $c = 2$. The right-hand side and the boundary conditions were chosen such that

$$u(x, y) = \frac{2}{\pi} \arctan(1000(-0.5x + y - 0.25))$$

is the exact solution of (1),(2).

First, as in Example 1, we apply the usual SDFEM (29) to (1),(2), with $\delta = h$. Next, we apply the p-Laplacian AV SGS method (11) to (1),(2), with $\mu = 1.0$, $\sigma = 1$, $p = 3$. Finally, we apply the bounded AV SGS model (19), with $\mu = 1$, $\sigma = 2$, $a(t) = -0.02 + 1/(1 + 49e^{-5.7t})$. The parameter choices for the two nonlinear AV methods have the same motivation as the corresponding ones in Example 1.

The surface plot and the contour lines for the SDFEM (29) are presented in Figure 8. Notice the undershooting and overshooting in the internal layer. The p-Laplacian AV SGS method (11) eliminates the undershooting and overshooting and spreads the internal layer over several elements (see Figure 9). The bounded AV SGS model (19) in Figure 10 yields improved results—the contour lines are tighter than those in Figure 9.

The numerical results corresponding to the three discretizations are summarized in Table 2. For different mesh-widths ($h = 1/16$, $h = 1/32$, $h = 1/64$, $h = 1/128$), Table 2 presents the L^2-norm of the error (denoted by $\|E\|_{L^2}$), and the $H1$-seminorm of the error (denoted by $|E|_{H1}$).

The bounded AV model performs consistently better than the p-Laplacian AV model: for $h = 1/128$ the L^2 norm of the error is three times smaller for the bounded AV model. The numerical results for both nonlinear AV models are better than those for the SDFEM in the $H1$-seminorm, but worse in the $L2$-norm.

Table 2. Example 2, norms of the errors for the three different discretizations, where "E" represents the error. The bounded, nonlinear AV SGS model performs consistently better than the p-Laplacian AV SGS model.

h	Norm	SDFEM	p-Laplacian AV	Bounded AV
$\frac{1}{16}$	$\|E\|_{L^2}$	0.152+0	0.321+0	0.209+0
	$\|E\|_{H1}$	0.700+1	0.556+1	0.609+1
$\frac{1}{32}$	$\|E\|_{L^2}$	0.108+0	0.250+0	0.144+0
	$\|E\|_{H1}$	0.132+2	0.113+2	0.112+2
$\frac{1}{64}$	$\|E\|_{L^2}$	0.633−1	0.189+0	0.867−1
	$\|E\|_{H1}$	0.191+2	0.180+2	0.165+2
$\frac{1}{128}$	$\|E\|_{L^2}$	0.255−1	0.134+0	0.360−1
	$\|E\|_{H1}$	0.158+2	0.196+2	0.152+2

5. CONCLUSIONS

This paper introduced a general, nonlinear SGS model, having bounded AV, for the numerical simulation of convection-dominated problems. As a first step in the validation of this new SGS model, we chose the linear setting of the convection-dominated convection diffusion problem (1),(2).

Indeed, there is little (if any) hope of understanding the effects of this nonlinear SGS model on the discretization of more general, nonlinear problems (such as the Navier-Stokes equations), without studying the effects on (1),(2) first.

We started with a careful mathematical (existence, uniqueness) and numerical (*a priori* error estimates) analysis of the new SGS model and the most common SGS model of Smagorinsky which uses a p-Laplacian regularization. Then, we tested these two nonlinear AV models on two challenging problems with sharp layers. The bounded, nonlinear AV model performed consistently better than the p-Laplacian AV model. To better assess the performance of these two nonlinear AV models, we also included numerical results for SDFEM, the most common approach for the discretization of the linear problem (1),(2).

These first results make the bounded, nonlinear AV SGS model a promising alternative to the popular Smagorinsky model in the numerical simulation of turbulent flows.

REFERENCES

1. B. Mohammadi and O. Pironneau, *Analysis of the K-Epsilon Turbulence Model*, John Wiley & Sons, Chichester, New York, (1994).
2. S.B. Pope, *Turbulent Flows*, Cambridge, (2000).
3. P. Sagaut, *Large Eddy Simulation for Incompressible Flows*, Springer, Berlin, (2002).
4. J. Smagorinsky, General circulation experiments with the primitive equation: I, The basic experiment, *Mon. Wea. Rev.* **91**, 216–241, (1963).
5. A.N. Brooks and T.J.R. Hughes, Streamline upwind/Petrov-Galerkin formulations for convection dominated flows with particular emphasis on the incompressible Navier-Stokes equations, *Comput. Methods Appl. Mech. Engrg.* **32**, 199–259, (1982).
6. U. Nävert, A finite element method for convection-diffusion problems, Ph.D. Thesis, Chalmers University of Technology, Göteborg (1982).
7. C. Johnson, U. Nävert and J. Pikäranta, Finite element methods for linear hyperbolic problems, *Comput. Methods Appl. Mech. Engrg.* **45**, 285–312, (1984).
8. K. Eriksson and C. Johnson, Adaptive streamline diffusion finite element methods for stationary convection-diffusion problems, *Math. Comput.* **60**, 167–188, (1993).
9. V. John, J.M. Maubach and L. Tobiska, Nonconforming streamline-diffusion-finite-element-methods for convection-diffusion problems, *Numer. Math.* **78**, 156–188, (1997).
10. H.G. Roos, M. Stynes and L. Tobiska, *Numerical Methods for Singularly Perturbed Differential Equations: Convection-Diffusion and Flow Problems*, Springer, Berlin, (1996).
11. Q. Du and M. Gunzburger, Finite element approximation for a Ladyzhenskaya model for stationary incompressible viscous flows, *SIAM J. Numer. Anal.* **27**, 1–19, (1990).
12. Q. Du and M. Gunzburger, Analysis of a Ladyzhenskaya model for incompressible viscous flow, *J. Math. Anal. Appl.* **155**, 21–45, (1991).
13. W.J. Layton, A nonlinear, subgridscale model for incompressible viscous flow problems, *SIAM J. Sci. Comput.* **17**, 347–357, (1996).
14. G. Minty, Monotone (nonlinear) operators in Hilbert space, *Duke Math. J.* **29**, 341–346, (1962).
15. J.L. Lions, *Quelques Méthodes de Résolution des Problèmes aux Limites Non Linéaires*, Dunod, Paris, (1969).
16. J. Barrett and W.B. Liu, Finite element approximation of degenerate quasilinear elliptic and parabolic problems, In *Numerical Analysis*, (Edited by D.F. Griffiths and G.A. Watson), Pitman Research Notes in Mathematics Series No. 303, pp. 1–16, Longman, (1994).
17. V. Girault and P.A. Raviart, *Finite Element Approximation of the Navier-Stokes Equations*, Springer-Verlag, Berlin, (1979).
18. M. Gunzburger, *Finite Element Methods for Viscous Incompressible Flow: A Guide to Theory, Practice, and Algorithms*, Academic Press, Boston, (1989).
19. M. Crouzeix and V. Thomée, The stability in L_p and W_p^1 of the L_2 projection onto finite element function spaces, *Math. Comput.* **48**, 521–532, (1987).
20. J.M. Maubach, *Iterative Methods for Nonlinear Partial Differential Equations*, C.W.I. Press, Amsterdam, (1991).
21. M.E. Cawood, V.J. Ervin, W.J. Layton and J.M. Maubach, Adaptive defect correction methods for convection dominated, convection diffusion problems, *J. Comput. Appl. Math.* **116**, 1–21, (2000).